Invisible metallic mesh

Dexin Ye[a,b], Ling Lu[b,1], John D. Joannopoulos[b,1], Marin Soljačić[b], and Lixin Ran[a,1]

[a]Laboratory of Applied Research on Electromagnetics, Zhejiang University, Hangzhou 310027, China; and [b]Department of Physics, Massachusetts Institute of Technology, Cambridge, MA 02139

Contributed by John D. Joannopoulos, January 14, 2016 (sent for review November 27, 2015; reviewed by Alexander Khanikaev, Frank Koppens, and Zheng Wang)

A solid material possessing identical electromagnetic properties as air has yet to be found in nature. Such a medium of arbitrary shape would neither reflect nor refract light at any angle of incidence in free space. Here, we introduce nonscattering corrugated metallic wires to construct such a medium. This was accomplished by aligning the dark-state frequencies in multiple scattering channels of a single wire. Analytical solutions, full-wave simulations, and microwave measurement results on 3D printed samples show omnidirectional invisibility in any configuration. This invisible metallic mesh can improve mechanical stability, electrical conduction, and heat dissipation of a system, without disturbing the electromagnetic design. Our approach is simple, robust, and scalable to higher frequencies.

invisible materials | scattering dark states | metamaterials

We introduce a solid material that is itself omnidirectionally invisible, possessing identical electromagnetic properties as air (i.e., not a cloak) at a desired frequency. Such a material could provide improved mechanical stability, electrical conduction, and heat dissipation to a system without disturbing incident electromagnetic radiation. One immediate application would be toward perfect antenna radomes. Unlike cloaks (1, 2), such a transparent and self-invisible material has yet to be demonstrated. Previous research (3–18) has shown that a single sphere or cylinder coated with plasmonic or dielectric layers can have a dark state with considerably suppressed scattering cross-section, due to the destructive interference between two resonances in one of its scattering channels. Nevertheless, a massive collection of these objects will have an accumulated and detectable disturbance to the original field distribution. Here we overcome this bottleneck by lining up the dark-state frequencies in different channels. Specifically, we derive analytically, verify numerically, and demonstrate experimentally that deliberately designed corrugated metallic wires can have record-low scattering amplitudes, achieved by aligning the nodal frequencies of the first two scattering channels. This enables an arbitrary assembly of these wires to be omnidirectionally invisible and the effective constitutive parameters nearly identical to air. Measured transmission spectra at microwave frequencies reveal indistinguishable results for all of the arrangements of the 3D-printed samples studied.

Although artificial dielectrics comprising conducting elements, now known as metamaterials, have been researched since the 1950s (19), such an air-like material simultaneously having unity permittivity and unity permeability has not been achieved. Our result is also fundamentally different from reflectionless materials such as perfect absorbers (20, 21) or Huygens metasurfaces (22–24). In contrast to these, our nonscattering material is both reflectionless and refractionless in arbitrary shapes under any incident angle.

This paper is organized as follows. First, we present the analytical solution of an ideal infinite corrugated thin conducting wire having an extremely low scattering width at a particular frequency. Materials made of such wires, having identical permittivity and permeability as air, would be invisible. Second, we design such an invisible medium using realistic materials modeled by full-wave simulations. Lastly, we describe the fabrication of a sample using this design and demonstrate its omnidirectional invisibility using microwave measurements.

Results

We begin by considering the plane wave scattering by an infinite cylindrical conducting wire with a radius r_1, as shown in Fig. 1*A* (when $r_2 = r_1$). When the incident electric field is parallel to the wire, the normalized scattering width $\sigma_{sca}/2r_1$ can be derived as $\sigma_{sca}/2r_1 = (2/k_0r_1)\sum_{n=-\infty}^{+\infty}\left|J_n(k_0r_1)/H_n^{(2)}(k_0r_1)\right|^2$ by the Mie solution (25) (*Derivation of the Scattering Width of the Infinite Corrugated Conducting Wire*), where J_n and $H_n^{(2)}$ denote a Bessel function and a Hankel function of the second kind, respectively. The normalized scattering width is plotted as the dashed gray line in Fig. 1*C*. At high frequencies, the scattering width σ_{sca} approaches a value equal to twice the wire diameter. There is only one resonance occurring at zero (dc) frequency, where the scattering width diverges. This can be explained using the resonance frequency $[\omega_0 = 1/(2\pi\sqrt{LC})]$ of inductance L and capacitance C of circuit elements. A thin long wire has an effective infinite inductance and capacitance ($L, C\to\infty$) (26, 27), leading to a zero resonance frequency ($\omega_0\to 0$).

It is known that a scattering dark state (scattering dip in frequency) universally exists between two resonances (scattering peaks), where the two resonances destructively interfere with equal amplitude but opposite phase in the same scattering and polarization channel (18). We can thus create such a scattering dark state by introducing a second resonance in the wire other than the one at dc. To introduce more resonances, we corrugate the wire by shrinking it periodically along the wire as shown in Fig. 1*A*. This corrugated wire consists of coaxial cylinders with different radii (r_1 and r_2) and heights (d_1 and d_2), where d_1 and d_2 are both far smaller than the free-space wavelength. Similar corrugated conducting wires have been proposed for guiding surface plasmon polaritons (28). The open volume can be filled with a low-loss material (dielectric constant ε_r) to improve the mechanical strength and increase the working wavelength, so the corrugations are more subwavelength and can be well described by the effective medium theory (29). Each open cylindrical

Significance

We introduce and demonstrate an invisible material—a solid composite possessing identical electromagnetic properties as air so that its arbitrarily shaped object neither reflects nor refracts light at any angle of incidence in free space. Such a material is self-invisible, unlike the cloaks for minimizing the scattering of other items. Invisible materials could provide improved mechanical stability, electrical conduction, and heat dissipation to a system, without disturbing the original electromagnetic design. One immediate application would be toward perfect antenna radomes.

Author contributions: D.Y., L.L., M.S., and L.R. designed research; D.Y. and L.L. performed research; D.Y., L.L., J.D.J., M.S., and L.R. analyzed data; J.D.J., M.S., and L.R. supervised the project; and D.Y., L.L., J.D.J., M.S., and L.R. wrote the paper.

Reviewers: A.K., Queens College, City University of New York; F.K., Institut de Ciencies Fotoniques; and Z.W., University of Texas at Austin.

The authors declare no conflict of interest.

[1]To whom correspondence may be addressed. Email: linglu@mit.edu, joannop@mit.edu, or ranlx@zju.edu.cn.

This article contains supporting information online at www.pnas.org/lookup/suppl/doi:10.1073/pnas.1600521113/-/DCSupplemental.

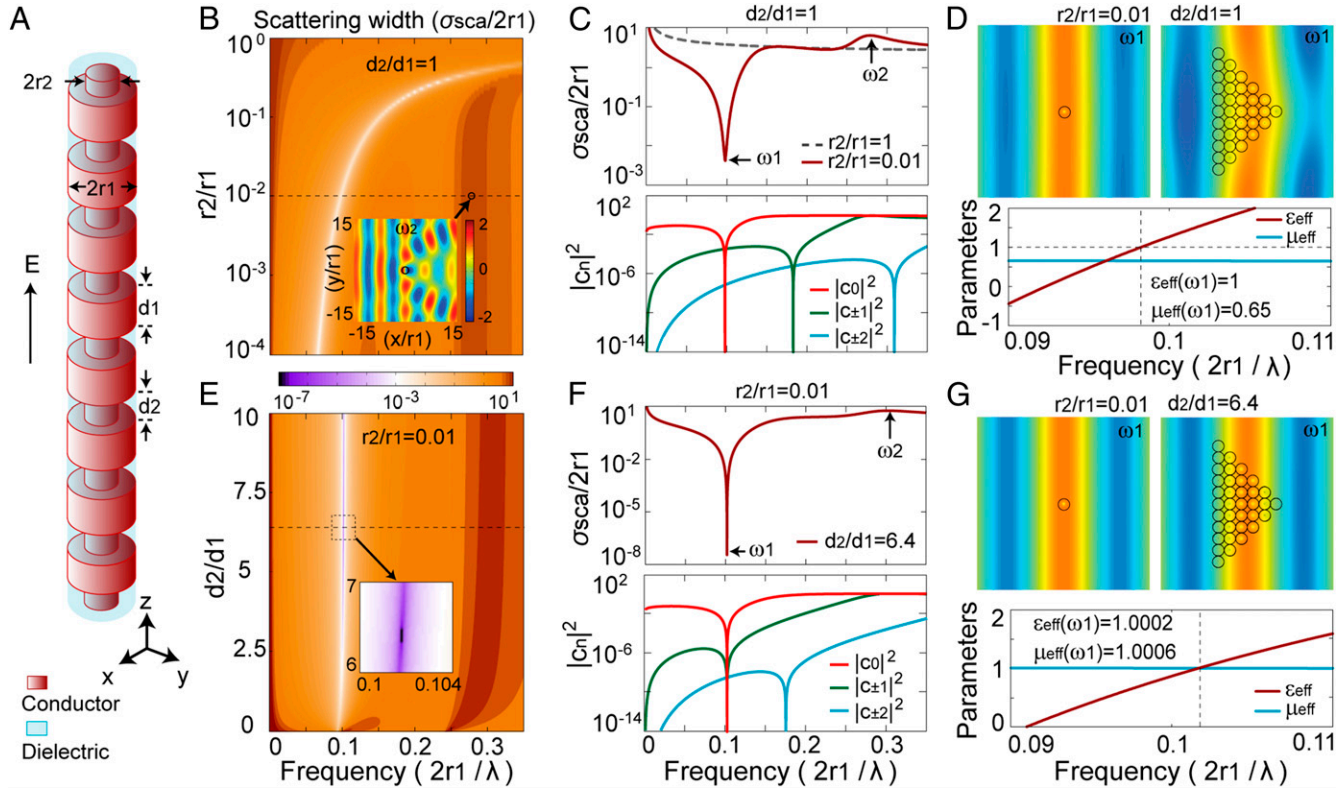

Fig. 1. Analytical solutions to wave scattering off corrugated conducting wires. (*A*) Geometry of a corrugated cylindrical conducting wire, whose open volumes are filled with a dielectric $\varepsilon_r = 6\varepsilon_0$. (*B*) The normalized total scattering widths for varying r_2/r_1 with subwavelength features d_1, d_2, set to $d_2/d_1 = 1$. (*Inset*) Total electric field around the wire under a unit-amplitude plane-wave incidence at normalized frequency $\omega_2 \approx 0.28$ for $r_2/r_1 = 0.01$. (*C, Top*) Total scattering widths for $r_2/r_1 = 0.01$ (red line) and $r_2/r_1 = 1$ (dashed gray line); the minimum scattering width is 4.8×10^{-3} at ω_1. (*C, Bottom*) Corresponding magnitudes of scattering coefficients ($|c_n|^2$) of different orders. The dips for zeroth-, first-, and second orders appear at different frequencies. (*D, Top Left*) Total electric field scattering off a single wire. (*D, Top Right*) Total electric field scattering off multiple closely arranged wires. The incident fields are unit-amplitude plane waves at frequency ω_1. (*D, Bottom*) Retrieved effective constitutive parameters of the closely arranged wires, $\varepsilon_{eff}(\omega_1) = 1$ and $\mu_{eff}(\omega_1) = 0.65$. (*E*) Normalized total scattering width as a function of d_2/d_1 with $r_2/r_1 = 0.01$. (*F, Top*) Total scattering width with $r_2/r_1 = 0.01$ and $d_2/d_1 = 6.4$; the minimum normalized scattering width is 3.5×10^{-8} at $\omega_1 = 0.1017$. (*F, Bottom*) Scattering coefficients, where the nodal frequencies of the zeroth- and first orders coincide at ω_1. (*G, Top Left*) Total electric field for a single wire. (*G, Top Right*) Total electric fields for multiple closely arranged wires. (*G, Bottom*) Retrieved effective constitutive parameters of the closely arranged wires, $\varepsilon_{eff}(\omega_1) = 1.0002$ and $\mu_{eff}(\omega_1) = 1.0006$.

space inside the wire forms a whispering gallery (WG) resonator; its spectrum and mode profiles are plotted in Fig. S1.

For such an infinite corrugated wire, its normalized scattering width can also be analytically derived, under the effective medium approximation, as (see *Derivation of the Scattering Width of the Infinite Corrugated Conducting Wire* for detailed derivation)

$$\sigma_{sca}/2r_1 = \frac{2}{k_0 r_1}\sum_{n=-\infty}^{+\infty}|c_n|^2, \qquad [1]$$

where $c_n = (J_n(k_0r_1)[J_n(k_{eff}r_2)Y_n'(k_{eff}r_1) - J_n'(k_{eff}r_1)Y_n(k_{eff}r_2)] - \eta_{eff}J_n'(k_0r_1)[J_n(k_{eff}r_2)Y_n(k_{eff}r_1) - J_n(k_{eff}r_1)Y_n(k_{eff}r_2)])/\eta_{eff}H_n^{2\prime}(k_0r_1)[J_n(k_{eff}r_2)Y_n(k_{eff}r_1) - J_n(k_{eff}r_1)Y_n(k_{eff}r_2)] - H_n^2(k_0r_1)[J_n(k_{eff}r_2)Y_n'(k_{eff}r_1) - J_n'(k_{eff}r_1)Y_n(k_{eff}r_2)]$, denotes the expanded nth-order scattering coefficient in Bessel (J_n and Y_n), Hankel functions ($H_n^{(2)}$), and their derivatives. Here $k_{eff} = \omega n_{eff} = \omega\sqrt{u_{||}^{eff}\times\varepsilon_z^{eff}} = \omega\sqrt{\varepsilon_r u_0}$, $\eta_{eff} = \sqrt{u_{||}^{eff}/\varepsilon_z^{eff}} = [d_2/(d_1+d_2)]\sqrt{u_0/\varepsilon_r}$, where $\varepsilon_z^{eff} = \varepsilon_r(d_1+d_2)/d_2$ and $\mu_{||}^{eff} = \mu_0 d_2/(d_1+d_2)$ are the effective permittivity and permeability of the corrugated volume ($r_2 \le \rho \le r_1$) derived in *Derivation of the Scattering Width of the Infinite Corrugated Conducting Wire*. We note that $J_0'(k_0r_1)$ approaches zero when k_0r_1 is a small number for a thin wire. So, the nodal frequency of c_0 has almost no dependence on η_{eff}, consequently independent of d_1 and d_2. Although the total scattering width $\sigma_{sca}/2r_1$ is the sum of all of the scattering coefficients $|c_n|^2$, $|c_n|^2$ is negligibly small when n is larger than k_0r_1 (~0.3 in our case) (30). As shown in Fig. 1*F*, $|c_2|^2$ is as small as 10^{-8}. So, the electromagnetic properties can mostly be determined by the first two scattering coefficients c_0 and c_1.

Shown as a white stripe in Fig. 1*B*, there will always exist a scattering dark state whose frequency ω_1 lies between those of the dc resonance and the first WG resonance ($\omega_2 \approx 0.28$) of the corrugated wire. In this plot, we vary the ratio of r_2/r_1 while fixing $d_1/d_2 = 1$ and $\varepsilon_r = 6$. In Fig. 1*C*, we decompose the total scattering width into individual orders and find that each order has its own zero-scattering frequency. Because the zeroth order is dominant, the dip in the total scattering corresponds to the nodal frequency of the zeroth scattering order c_0. The same mechanism enabled previous studies on transparent (cloaking) wires (3–9), invisible particles (10–18), or scattering dark states (31–34).

However, the vanishing of $c_0 = 0$ is not enough to make a collection of these wires invisible; the total scattering amplitude is not small enough when $c_1 \neq 0$. In Fig. 1*D*, we show the obvious distortion of a scattered wave by a set of these wires packed closely. For a better understanding, we also show the effective constitutive parameters of an array of such wires at the bottom of Fig. 1*D*, using a homogenization approach (35). At ω_1, $\varepsilon_{eff} = 1$ and $\mu_{eff} = 0.65$. Although the effective permittivity of the material ε_{eff} is 1 (the same as that of free space), $\mu_{eff} \neq 1$. By solving the Mie scattering solutions for a homogeneous dielectric thin wire (*Scattering of a Homogeneous Infinite Dielectric Cylinder with*

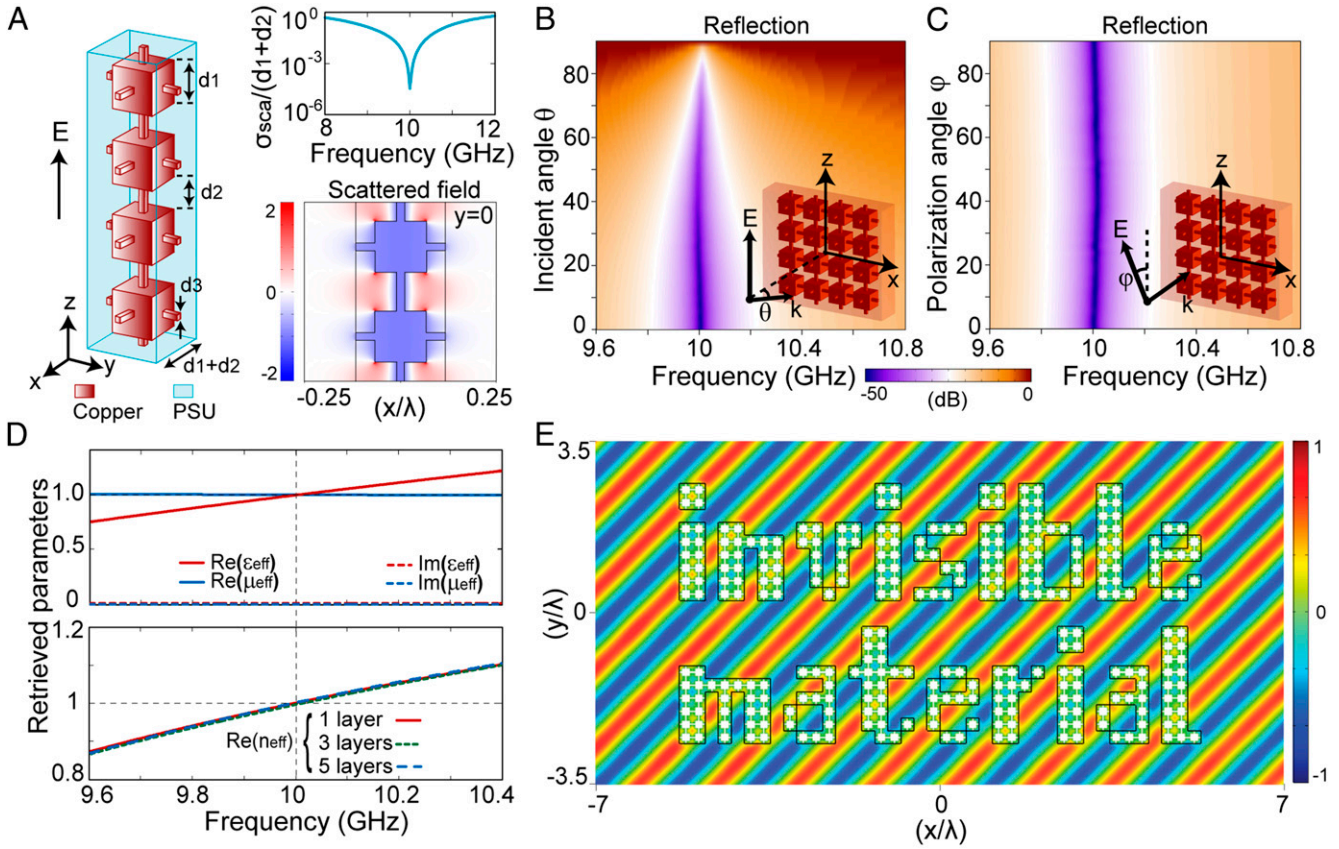

Fig. 2. Numerical results of the invisible material made of corrugated metallic wires. (*A*, *Left*) Geometry of a modified wire, composed of corrugated conducting square wire embedded in a dielectric with $\varepsilon_r = 3$ and a loss tangent of 0.0013. (*A*, *Top Right*) Normalized scattering width (5×10^{-5} at 10 GHz) under a normal plane-wave incidence along the *x* axis with the unit-amplitude electric field polarized along the *z* axis. (*A*, *Bottom Right*) Scattered electric field around the corrugated wire at 10 GHz. (*B*) Simulated reflectance spectra (S_{11}) for one layer of wires with respect to the angle of incidence. (*C*) Simulated reflectance spectra with respect to the polarization angle. (*D*) Retrieved effective parameters of the solid slab composed of closely arranged corrugated wires with different layer thickness. For the one-layer slab, $\varepsilon_{eff} = 0.9999 + 0.006i$, $\mu_{eff} = 1$, and the refractive index $n_{eff} \sim 1 + 0.003i$ at 10 GHz. (*E*) Steady-state electric field distribution under an oblique plane-wave incidence at 10 GHz upon an invisible material-shaped structure composed of the designed wires. The electric field is polarized along the *z* axis.

Radius r), we show that $c_0 = 0$ requires $\varepsilon = 1$ and $c_1 = 0$ requires $\mu = 1$. Because the nodal frequencies of c_0 and c_1 in general occur at different frequencies for a single element, $\varepsilon = \mu = 1$ cannot be satisfied simultaneously for an assembly of them. This is why no transparently invisible metamaterial has been reported to date.

Now, we tune the nodal frequency of c_1 to coincide with that of c_0 for an individual wire (i.e., $c_0 = c_1 = 0$ at the same frequency), which results in a further decrease of the total scattering amplitude by 5 orders of magnitude to a negligible value. Consequently, $\varepsilon_{eff} \approx \mu_{eff} \approx 1$ for an arbitrary assembly of such wires. We achieve this by tuning the geometry of the corrugation. We have seen that c_0 is almost independent of d_2/d_1, whereas the c_i ($i > 0$) have a strong dependence on d_2/d_1. For example, the white line (nodal frequency of c_0) in Fig. 1*E* is almost a straight vertical line that does not change with d_2/d_1. So, by varying d_2/d_1, we can freely tune the nodal frequency of c_1 toward that of c_0. Starting with the configuration in Fig. 1*B* where r_2/r_1 is fixed at 0.01, we tune the ratio of d_2/d_1 from 1 to ~6.4 in Fig. 1*E*. The nodal frequencies of c_0 and c_1 coincide and the total scattering width decreases by 5 orders of magnitude to a record-low scattering width of 3.5×10^{-8} (which eventually will be limited by material losses in experiments). At the same time, μ_{eff} increases from 0.65 to 1.0006. Consequently, the wave experiences no distortion after impinging on closely arranged wires in Fig. 1*G*, compared with Fig. 1*D*. (More results are provided in Fig. S2 for different arrangements of the wires.) This means arbitrary composites of such wires should be practically invisible. We emphasize that such an alignment of nodal frequencies can robustly occur at any frequency by tuning r_2/r_1 and d_2/d_1 (Fig. S3).

For ease of fabrication, we modify the cylinders in the wire into cubes in Fig. 2*A*. We connect the cubes with thin square-shaped rods symmetrical in the *x*-, *y*-, and *z* directions. This makes the original wire structure cubic symmetric, which removes the previous constraint that the field polarization has to be vertical. This conducting skeleton is embedded in a low-loss dielectric. Such a modified construction, still being subwavelength, has no qualitative change in its scattering properties from the corrugated wires studied analytically in Fig. 1. We performed full-wave simulations on this rectangular wire structure using CST Microwave Studio. The dimensions are $d_1 = 4$ mm, $d_2 = 3$ mm, and $d_3 = 0.6$ mm. The conductor is copper with a conductance of 5.986×10^7 S/m, and the dielectric is polysulfone (PSU) with dielectric constant of 3 and loss tangent of 0.0013. Shown in Fig. 2*A*, the invisible frequency occurs at around 10 GHz with a normalized scattering width as low as 5×10^{-5}. The scattered electric field (difference between fields with and without the wire) is almost all localized inside the wire, consistent with the near-zero scattering width. The opposite phase at different sections along the wire leads to the cancellation of the outgoing waves in the far field. We note that this structure has a low loss at the invisible frequency that is spectrally far away from the resonances.

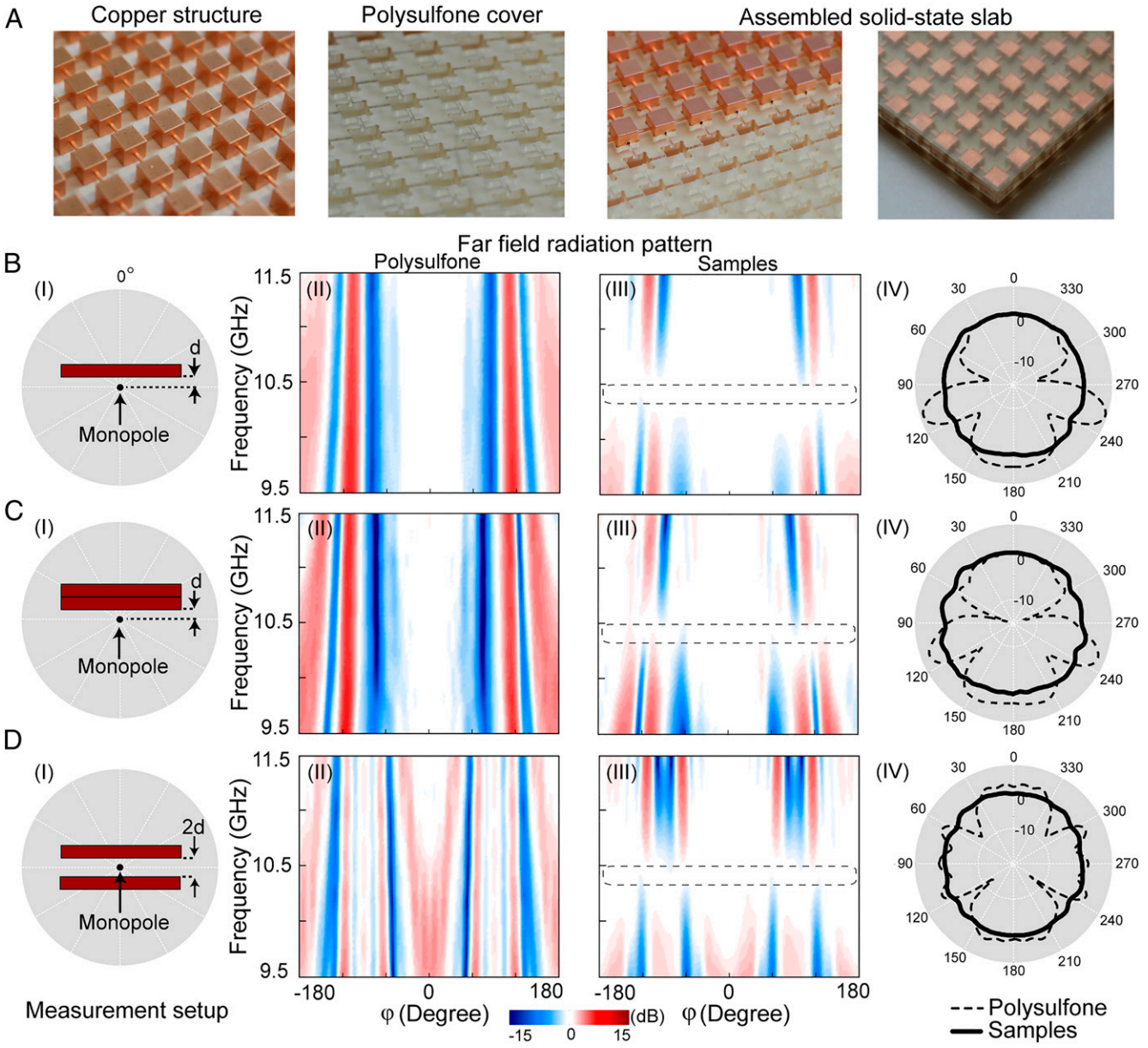

Fig. 3. Experimental measurements of the fabricated samples. (*A*) Slab samples composed of closely arranged corrugated wires. (*B*) Experimental far-field radiation pattern measured for a single layer of slab. (*B*, *I*) Experimental setup; (*B*, *II* and *III*) measured field amplitude for an identical PSU slab and the sample slab; and (*B*, *IV*) radiation pattern. (*C*) Measurement for two stacked layers. (*D*) Measurement for two spaced slabs. *d* is 20 mm. The radiation patterns in polar coordinates are plotted with data at 10.4 GHz.

When the wires are packed into a single 2D plane as in Fig. 2*B* (*Inset*), the reflection spectra off the mesh sheet show hardly any dispersion in either the polarization direction or incident angle, as long as the incident electric field is parallel to the sample plane (*S*-polarized). The reflection is lower than −45 dB for normal incidence and remains below −30 dB for the incident angle of 80°. The performance is also independent of the polarization angle as shown in Fig. 2*C*, a result of its in-plane geometry. Again, we show the effective constitutive parameters of this layer of wires in Fig. 2*D* (*Top*). At 10 GHz, $\varepsilon_{eff} = 0.9999 + 0.006i$ and $\mu_{eff} = 1$. Accordingly, the real part of its effective refractive index is almost unity and it is nearly independent of the number of layers as shown in Fig. 2*D* (*Bottom*). So, we can conclude that arbitrary arrangements of this mesh will be invisible as long as the electric field is parallel to the metallic wire within the beam width. To further illustrate this unique air-like material, we performed full-wave simulations on a network of wires with selected wires to represent the words "invisible material" shown in Fig. 2*E*. Under an oblique incidence of plane wave at 10 GHz, the steady-state total electric fields in air stay undisturbed, showing a perfect invisibility. Animation of the electric field propagation can be found in Movies S1–S4.

As shown in Fig. 3*A*, the sample was fabricated by sandwiching the copper-connected cubes between two pieces of PSU covers. The dimensions of the samples are $217 \times 252 \times 7$ mm^3 ($31 \times 36 \times 1$ in periods). To make the copper structure, we first 3D-print a plastic array of the connected cubes using stereolithography (material: Accura 60). Then, a metal sputtering process was used to coat the surfaces of the plastic array with 50 μm of copper film that is well above the skin depth (0.64 μm) at 10 GHz. The two PSU

cover layers were machined with grooves and square openings so the copper structure could be embedded tightly inside.

In the measurements, three sets of sample configurations were studied. In the first configuration (Fig. 3*B*), one layer of the assembled slab was placed on a rotation stage spinning around a small monopole antenna with a separation distance of d (20 mm) from the slab, shown in Fig. 3 *B*, *I*. We choose this subwavelength separation to observe a strong redistribution of fields due to the sample. A wideband signal was fed into the monopole, and a wideband receiving lens antenna was placed at the other side to detect the far-field radiation patterns by measuring transmission amplitudes S_{21} (S parameter) using an Agilent E8361A network analyzer. All transmission amplitudes are normalized by the reference transmission signal when the sample is removed. For comparison, a reference measurement was performed by replacing the sample with a PSU slab of the same size. Shown in Fig. 3 *B*, *II*, the radiation pattern of the PSU sample is strongly directional for all frequencies. But, for the designed sample shown in Fig. 3 *B*, *III*, there exists a frequency range around 10.4 GHz where the radiation pattern is almost a circle within a 7.2% relative bandwidth where the scattering amplitudes are less than ±1 dB. For a direct comparison in Fig. 3 *B*, *IV*, we plot the transmission amplitudes in angular polar coordinates for both the sample and the reference at 10.4 GHz, validating the omnidirectional invisibility of the sample. Although fabrication imperfections inevitably degrade the performance and shift the operating frequency from 10 to 10.4 GHz, the measurement results agree with our analytic and numerical results.

In the second configuration (Fig. 3*C*), two slab samples were stacked together as a thicker one. Equivalent sets of measurements were performed as those for the first configuration. In the third configuration (Fig. 3*D*), the two slab samples were separated on the two sides of the source antenna. In both configurations, similar results were obtained as those of the first configuration. The above results confirm that the fabricated sample is omnidirectionally invisible regardless of its geometry.

Discussion

In conclusion, we have demonstrated the ability to construct invisible microwave materials out of corrugated wires with record-low scattering width. Our analytical analyses, numerical simulations, and experimental measurements are all consistent. We hope this work will inspire new technological applications, one important example being the construction of perfect antenna radomes. Objects can also be cloaked inside the metallic cubes. The proposed approach is simple, robust, and scalable to higher frequencies using low-loss metals. Based on the general ability to control the frequency dispersions by multiple resonant structures (36), it should be possible to design wider-bandwidth materials invisible to both polarizations using our approach.

ACKNOWLEDGMENTS. We thank Zhiyu Wang, Hongshen Chen, Yichen Shen, and Chia Wei Hsu for discussions. This work is supported by the National Natural Science Foundation of China under Grants 61401393 and 61131002, and the China Postdoctoral Science Foundation under Grant 2014M550325. J.D.J. was supported in part by the US Army Research Office through the Institute for Soldier Nanotechnologies under Contract W911NF-13-D-0001. L.L. was supported in part by the Materials Research Science and Engineering Center Program of the National Science Foundation under Award DMR-1419807. M.S. and L.L. (analysis and reading of the manuscript) were supported in part by the Massachusetts Institute of Technology (MIT) Solid-State Solar-Thermal Energy Conversion Center and Energy Frontier Research Center of the Department of Energy under Grant DE-SC0001299.

1. Pendry JB, Schurig D, Smith DR (2006) Controlling electromagnetic fields. *Science* 312(5781):1780–1782.
2. Chen H, et al. (2013) Ray-optics cloaking devices for large objects in incoherent natural light. *Nat Commun* 4:2652.
3. Irci E, Ertürk VB (2007) Achieving transparency and maximizing scattering with metamaterial-coated conducting cylinders. *Phys Rev E Stat Nonlin Soft Matter Phys* 76(5 Pt 2):056603.
4. Edwards B, Alù A, Silveirinha MG, Engheta N (2009) Experimental verification of plasmonic cloaking at microwave frequencies with metamaterials. *Phys Rev Lett* 103(15):153901.
5. Tretyakov S, Alitalo P, Luukkonen O, Simovski C (2009) Broadband electromagnetic cloaking of long cylindrical objects. *Phys Rev Lett* 103(10):103905.
6. Valagiannopoulos CA, Alitalo P (2012) Electromagnetic cloaking of cylindrical objects by multilayer or uniform dielectric claddings. *Phys Rev B* 85(11):115402.
7. Valagiannopoulos CA, Alitalo P, Tretyakov SA (2014) On the minimal scattering response of PEC cylinders in a dielectric cloak. *IEEE Antenn Wirel Pr* 13:403–406.
8. Rybin MV, Filonov DS, Belov PA, Kivshar YS, Limonov MF (2015) Switching from visibility to invisibility via Fano resonances: Theory and experiment. *Sci Rep* 5:8774.
9. Wang H, Zhang X (2009) Achieving multifrequency transparency with cylindrical plasmonic cloak. *J Appl Phys* 106(5):053302.
10. Alù A, Engheta N (2005) Achieving transparency with plasmonic and metamaterial coatings. *Phys Rev E Stat Nonlin Soft Matter Phys* 72(1 Pt 2):016623.
11. Kerker M (1975) Invisible bodies. *J Opt Soc Am* 65(4):376–379.
12. Chew H, Kerker M (1976) Abnormally low electromagnetic scattering cross-sections. *J Opt Soc Am* 66(5):445–449.
13. Alu A, Engheta N (2007) Cloaking and transparency for collections of particles with metamaterial and plasmonic covers. *Opt Express* 15(12):7578–7590.
14. Alù A, Engheta N (2008) Multifrequency optical invisibility cloak with layered plasmonic shells. *Phys Rev Lett* 100(11):113901.
15. Evangelou S, Yannopapas V, Paspalakis E (2012) Transparency and slow light in a four-level quantum system near a plasmonic nanostructure. *Phys Rev A* 86(5):053811.
16. Alù A, Engheta N (2007) Plasmonic materials in transparency and cloaking problems: Mechanism, robustness, and physical insights. *Opt Express* 15(6):3318–3332.
17. Alù A, Engheta N (2008) Effects of size and frequency dispersion in plasmonic cloaking. *Phys Rev E Stat Nonlin Soft Matter Phys* 78(4 Pt 2):045602.
18. Hsu CW, DeLacy BG, Johnson SG, Joannopoulos JD, Soljačić M (2014) Theoretical criteria for scattering dark states in nanostructured particles. *Nano Lett* 14(5): 2783–2788.
19. Brown J (1953) Artificial dielectrics having refractive indices less than unity. *Proc IEE* 100IV:51.
20. Landy NI, Sajuyigbe S, Mock JJ, Smith DR, Padilla WJ (2008) Perfect metamaterial absorber. *Phys Rev Lett* 100(20):207402.
21. Ye D, et al. (2012) Towards experimental perfectly-matched layers with ultra-thin metamaterial surfaces. *IEEE Trans Antenn Propag* 60(11):5164–5172.
22. Pfeiffer C, Grbic A (2013) Metamaterial Huygens' surfaces: tailoring wave fronts with reflectionless sheets. *Phys Rev Lett* 110(19):197401.
23. Decker M, et al. (2015) High-efficiency dielectric Huygens' surfaces. *Adv Opt Mater* 3(6):813–820.
24. Staude I, et al. (2013) Tailoring directional scattering through magnetic and electric resonances in subwavelength silicon nanodisks. *ACS Nano* 7(9):7824–7832.
25. Kong JA (2000) *Electromagnetic Wave Theory* (EMW Publishing, Cambridge, MA).
26. Maxwell JC (1878) On the electrical capacity of a long narrow cylinder and of a disk of sensible thickness. *Proc Lond Math Soc* IX:94–101.
27. Pendry JB, Holden AJ, Stewart WJ, Youngs I (1996) Extremely low frequency plasmons in metallic mesostructures. *Phys Rev Lett* 76(25):4773–4776.
28. Maier SA, Andrews SR, Martín-Moreno L, García-Vidal FJ (2006) Terahertz surface plasmon-polariton propagation and focusing on periodically corrugated metal wires. *Phys Rev Lett* 97(17):176805.
29. Smith DR, Schultz S, Markos P, Soukoulis CM (2002) Determination of effective permittivity and permeability of metamaterials from reflection and transmission coefficients. *Phys Rev B* 65(19):195104–195108.
30. Bohren C, Huffman DR (1983) *Absorption and Scattering of Light by Small Particles* (Wiley, New York).
31. Wu X, Gray SK, Pelton M (2010) Quantum-dot-induced transparency in a nanoscale plasmonic resonator. *Opt Express* 18(23):23633–23645.
32. Zengin G, et al. (2013) Approaching the strong coupling limit in single plasmonic nanorods interacting with J-aggregates. *Sci Rep* 3:3074.
33. Forestiere C, Dal Negro L, Miano G (2013) Theory of coupled plasmon modes and Fano-like resonances in subwavelength metal structures. *Phys Rev B* 88(15):155411.
34. Giannini V, Francescato Y, Amrania H, Phillips CC, Maier SA (2011) Fano resonances in nanoscale plasmonic systems: A parameter-free modeling approach. *Nano Lett* 11(7): 2835–2840.
35. Chen X, Grzegorczyk TM, Wu BI, Pacheco J, Jr, Kong JA (2004) Robust method to retrieve the constitutive effective parameters of metamaterials. *Phys Rev E Stat Nonlin Soft Matter Phys* 70(1 Pt 2):016608.
36. Ye D, et al. (2013) Ultrawideband dispersion control of a metamaterial surface for perfectly-matched-layer-like absorption. *Phys Rev Lett* 111(18):187402.
37. Piefke G (1959) The transmission characteristics of a corrugated guide. *IEEE Trans Antenn Propag* 7(5):183–190.
38. Wait JR (1955) Scattering of a plane wave from a circular dielectric cylinder at oblique incidence. *Can J Phys* 33(5):189–195.